A Comparison of Functional Models for the Subgrid-scale Stress Tensor in LES of a Coaxial Turbulent Jet

Jean Monteiro de Pinho

IFSC, Federal Institute of Santa Catarina, Euclides Hack St, 1603, 89820-000, Xanxerê, SC, Brazil

jean.pinho@ifsc.edu.br

André Rodrigues Muniz

UFRGS, Department of Chemical Engineering, Rua Engenheiro Luiz Englert, s/n, 90040-040, Porto Alegre, RS, Brazil

munizeq@gmail.com

***Abstract.** Large Eddy Simulation (LES) is a promising technique to simulate turbulent flows, based on the elimination of flow scales smaller than a characteristic length, and direct resolution of the largest scales. There is a variety of subgrid-scale models available in the literature to describe the turbulence in small scales, with different levels of complexity and computational cost. Although many advances have been achieved since the development of the LES technique, there is still no consensus on a definitive subgrid model for generic use in engineering applications. The objective of this work is to analyze the effect of subgrid modeling in LES of turbulent coaxial jets. Simulations were carried out for a test problem using the Smagorinsky, Germano and Velocity Structure function models, and results were compared with experimental data from the literature. The best results for average properties were found with the Smagorinsky model with an optimal ad hoc coefficient, while the dynamic model of Germano was the one that best described the turbulent features. These results show that this type of comparative analysis is of fundamental importance to obtain reliable results when addressing new problems.*

1. INTRODUCTION

Turbulence is a phenomenon present in most flows observed in nature and in engineering applications. Turbulent flows are unstable and their properties exhibit fluctuations that are time and space dependent, and one of their most striking feature is the multiplicity of scales. The Large Eddy Simulation (LES) is a promising technique to simulate turbulent flows, based on the elimination of all scales of the flow smaller than a characteristic length scale Δ. It allows capturing the anisotropic turbulence that occurs in the large scales by directly solving the intermediate scales, while the small scales (whose behavior is no significantly influenced by the geometry of the problem (Tennekes and Lumley, 1972)) are described by homogeneous isotropic turbulence models. The separation of the scales is performed through the proper application of a low-pass filter in the system of equations, which results in the so called LES equations, able to describe the flow in the largest scales (Lesieur *et al.*, 2005). In terms of computational cost, LES is an intermediate methodology between the other techniques traditionally used in simulation of turbulent flows (DNS and RANS).

In the framework of LES, there are a variety of models to describe the interaction between the solved and unsolved scales, called *subgrid-scale* (SGS) models, with different mathematical and physical foundations and levels of complexity. Examples are the Smagorinsky model (Smagorinsky, 1963), the dynamic model of Germano *et al.* (DSGS) (Germano *et al.*, 1991) and the Velocity Structure Functions (VSF) (Métais and Lesieur, 1992). The analysis of the performance of existing models is an important step for their application in problems of interest and in the development of new methods (Löffler *et al.*, 2008).

Coaxial turbulent jets are relevant in several practical applications in combustion and propulsion. Lele and collaborators (Bodony and Lele, 2008; Brès and Lele, 2019) have presented reviews on the application of LES to simulate coaxial turbulent jets, showing that there is an interaction between the numerical method and the SGS modeling, and that there is no consensus in the literature about the most suitable SGS model for such purpose. In this sense, the objective of this work is to carry out a comparative analysis of the effect of subgrid modeling on LES of turbulent coaxial jets of constant density. The Smagorinsky, DSGS and VSF subgrid-scale models were employed in the LES of a benchmark problem, and results for the average velocities and turbulence intensities are compared to experimental data (Amielh *et al.*, 1996; Djeridane *et al.*, 1996). The simulations are carried out with the PMLES code (Pinho and Muniz, 2020), designed to run on a hybrid CPU-GPU architecture, allowing running simulations in a computational domain with 1×10^8 points using a single computing node in a GPU card.

2. METHODOLOGY

2.1 LES Modeling

In the LES methodology, the filtering operation is responsible to separate mathematically a variable $f(\mathbf{x}, t)$ in two components: one related to the large scales of the flow to be solved $\overline{f}(\mathbf{x}, t)$, and other to the small scales to be modeled $f'(\mathbf{x}, t)$ (also called subgrid scales):

$$f(\mathbf{x}, t) = \overline{f}(\mathbf{x}, t) + f'(\mathbf{x}, t) \tag{1}$$

This approach is also known as Leonard decomposition (Pope (2000)). The filtering consists of the convolution of the variable to be filtered on the filter function G

$$\overline{f}(\mathbf{x}, t) = \int_D f(\mathbf{x}', t) G(\mathbf{x} - \mathbf{x}' : t) d\mathbf{x} \tag{2}$$

where D is the domain on which the operation must be performed.

The filtering process aims to eliminate or smooth out fluctuations that are smaller than the predefined cutoff wave number. The challenge is to find a good balance between filter size, accuracy and computational cost. LES modeling involves two filtering processes: a dimensional filter (δ) and a grid filter (Δ) (Kuo and Acharya, 2012). The phenomena that occurs in a scale smaller than the grid filter cannot be captured by any of the filters, and they are modeled. The scales smaller than grid filter (Δ) are called *sub-grid scales*.

LES modeling allows using either explicit or implicit filters, provided that they represent the properties of the sub-grid terms. Most applications in LES use the constant volumetric filter, also called top-hat filter (Silva Freire *et al.*, 2002)

$$G(\mathbf{x}) = \begin{cases} 1/\Delta^3, \text{if } |x_i| \leq \Delta/2, \ \ i = 1, 2, 3; \\ 0, \text{otherwise}, \end{cases} \tag{3}$$

which is an implicit filter, considering that the characteristic size of the filter is equal to the mesh spacing length. In this case the filtering and differentiation operation commute. This approach is also called Schumann filtering (Huai, 2006) and was used in this work.

In the present work, Favre averaging was applied to the conservation equations. A filtered variable f is defined as:

$$\widetilde{f} = \frac{\overline{\rho f}}{\overline{\rho}}, \tag{4}$$

and the following relations are verified (Kuo and Acharya, 2012):

$$\overline{\rho u_i} = \overline{\rho} \widetilde{u_i}, \tag{5}$$
$$\overline{\rho u_i u_j} = \overline{\rho} \widetilde{u_i u_j}. \tag{6}$$

A variable can be then decomposed into its Favre filtered component $\widetilde{f}$ and its subgrid component f':

$$f(\mathbf{x}, t) = \widetilde{f}(\mathbf{x}, t) + f'(\mathbf{x}, t). \tag{7}$$

This procedure is applied to the velocity field. Variables whose effects of the density are inherent to the measurement process, such as pressure, stress tensors and the specific mass itself, do not need to be filtered by the Favre average. For these variables, the conventional time averaging can be used (Kuo and Acharya, 2012). As a result of the filtering process, the momentum equation becomes

$$\frac{\partial (\overline{\rho u_i})}{\partial t} + \frac{\partial (\overline{\rho u_i u_j})}{\partial x_j} = \frac{\partial \overline{p}}{\partial x_i} + \mu \left(\frac{\partial^2 \overline{u_i}}{\partial x_j{}^2} + \frac{\partial^2 \overline{u_j}}{\partial x_i{}^2} \right) \tag{8}$$

Details of the application of the filter in the momentum equation can be seen in Moint *et al.* (Moin *et al.*, 1991) and Kuo and Acharya (Kuo and Acharya, 2012). The nonlinear term of the filtered equation (Eq. 8) results in a product of two filtered variables, making their solution unfeasible. This nonlinear term can be treated using the Leonard decomposition in terms of the Favre filter (Sagaut, 2006), as defined in Eqs. 1 and 4, so that

$$\overline{\rho u_i u_j} \equiv \overline{\rho (\widetilde{u_i} + u_i')(\widetilde{u_j} + u_j')}$$
$$\overline{\rho u_i u_j} = \overline{\rho \widetilde{u_i}\widetilde{u_j}} + \overline{\rho \widetilde{u_i} u_j'} + \overline{\rho u_i' \widetilde{u_j}} + \overline{\rho u_i' u_j'}. \tag{9}$$

Adding and subtracting the term $\overline{\rho} \widetilde{u_i}\widetilde{u_j}$, and replacing in Eq. 8 we have

$$\frac{\partial (\overline{\rho u_i})}{\partial t} + \frac{\partial (\overline{\rho} \widetilde{u_i}\widetilde{u_j})}{\partial x_j} = \frac{\partial \overline{p}}{\partial x_i} + \mu \left(\frac{\partial^2 \widetilde{u_i}}{\partial x_j{}^2} + \frac{\partial^2 \widetilde{u_j}}{\partial x_i{}^2} \right) - \frac{\partial}{\partial x_j} \left[\overline{\rho \widetilde{u_i}\widetilde{u_j}} - \overline{\rho} \widetilde{u_i}\widetilde{u_j} + \overline{\rho \widetilde{u_i} u_j'} + \overline{\rho u_i' \widetilde{u_j}} + \overline{\rho u_i' u_j'} \right]. \tag{10}$$

The subgrid-scale stress tensor $(\sigma_{ij})_{sgs}$ is then defined as

$$(\sigma_{ij})_{sgs} = \overline{\rho u_i u_j} - \overline{\rho}\widetilde{u}_i\widetilde{u}_j \tag{11}$$

$$(\sigma_{ij})_{sgs} = \overline{\rho}\left(\widetilde{u_i u_j} - \widetilde{u}_i\widetilde{u}_j\right), \tag{12}$$

$$(\sigma_{ij})_{sgs} = \overline{\rho\widetilde{u}_i\widetilde{u}_j} - \overline{\rho}\widetilde{u}_i\widetilde{u}_j + \overline{\rho}\left(\overline{\widetilde{u}_i u_j{}'} + \overline{u_i{}'\widetilde{u}_j}\right) + \overline{\rho u_i{}'u_j{}'}$$

$$(\sigma_{ij})_{sgs} = L_{i,j} + C_{i,j} + R_{i,j} \tag{13}$$

where $L_{i,j}$ is the Leonard-stress tensor that represents the interaction between the resolved scales (that results in the subgrid contributions), $C_{i,j}$ is the Cross-stress tensor that represents the interaction between the resolved scales and the unresolved scales, and $R_{i,j}$ is the Reynolds-stress tensor, that represents the interaction between the unresolved small scales. The conservation equations can be then written as follows:

$$\frac{\partial\overline{\rho}}{\partial t} + \frac{\partial\overline{\rho}\widetilde{u}_i}{\partial x_i} = 0; \tag{14}$$

$$\frac{\partial\left(\overline{\rho}\widetilde{u}_i\right)}{\partial t} + \frac{\partial\left(\overline{\rho}\widetilde{u}_i\widetilde{u}_j\right)}{\partial x_j} = -\frac{\partial\overline{p}}{\partial x_i} + \frac{\partial(\sigma_{ij})_{sgs}}{\partial x_i} + \frac{1}{Re}\left(\frac{\partial^2\widetilde{u}_i}{\partial x_j{}^2} + \frac{\partial^2\widetilde{u}_j}{\partial x_i{}^2}\right). \tag{15}$$

An ideal SGS model should provide a correct description of the interaction between the solved large scales and unsolved small scales, allowing the flux of kinetic energy between the scales in both directions (forward and reverse energy cascades). In this work, the three tested models, are classified as functional models (Sagaut, 2006) and are based on the hypothesis that the action of the sub-grid scales on the solved scales is essentially of energetic nature, as a eddy viscosity (Schmitt, 2007). The concept of eddy viscosity assumes that the mechanism for energy transfer from the solved scales to the subgrid ones is analogous to the molecular mechanism. In this case, the subgrid stress tensor can be written as:

$$\sigma_{ij}^{sgs} = -\nu_t\left(\frac{\partial\widetilde{u}_i}{\partial x_j} + \frac{\partial\widetilde{u}_j}{\partial x_i}\right) + \frac{2}{3}\nu_t\frac{\partial\widetilde{u}_k}{\partial x_k}\delta_{ij}, \tag{16}$$

Since the study of acoustic interactions and compressibility effects are outside the scope of this work, Eq. 16 does not include the isotropic portion (Pierce and Moin, 2004; Pierce, 2001). The combination of the eddy viscosity μ_t with the molecular viscosity can be used to define a dimensionless effective viscosity $\mu_e = \frac{\mu+\mu_t}{\mu}$, allowing the Eq. 15 to be rewritten as

$$\frac{\partial\left(\widetilde{\rho}\widetilde{u}_i\right)}{\partial t} + \frac{\partial\left(\widetilde{\rho}\widetilde{u}_i\widetilde{u}_j\right)}{\partial x_j} = -\frac{\partial\overline{p}}{\partial x_i} + \frac{\mu_e}{Re}\left(\frac{\partial^2\widetilde{u}_i}{\partial x_j{}^2} + \frac{\partial^2\widetilde{u}_j}{\partial x_i{}^2}\right). \tag{17}$$

The three methodologies used to compute the SGS stress tensor are briefly presented in the following subsections.

2.1.1 Smagorinsky Model

The Smagorinsky model (Smagorinsky, 1963) is the most traditional SGS model, and despite its simplicity, it provides good quality results for many problems. According to this model, the eddy viscosity is evaluated as

$$\mu_t = \rho(C_s\Delta_S)^2|\widetilde{S}|, \tag{18}$$

where

$$|\widetilde{S}| = \sqrt{2\widetilde{S}_{ij}\widetilde{S}_{ij}} \tag{19}$$

$$\Delta_S = \sqrt[3]{\Delta x\Delta y\Delta z}, \tag{20}$$

being $\widetilde{S}_{ij}$ is the strain rate tensor and C_s the so called Smagorinsky constant. The positive characteristics of the Smagorinsky model are the easy implementation, lower computational cost and satisfactory results for a large number of engineering applications. Their main weaknesses include the excessive dissipation near surfaces, the inability of reproducing the reverse energy cascade, and the necessity of defining the *ad hoc* constant C_s, according to the flow characteristics. Large values of C_s may introduce significant dissipation on the model, smoothing the turbulent features of the flow. On the other hand, the use of a small value for C_s may destabilize the solution procedure. There is no consensus about a general value of C_s to be used in the simulations of shear flows, and a wide range of values has been suggested. In this work, we use $C_s = 0.060$, which was the value that led to results (obtained with the PMLES solver) exhibiting the best agreement with the experimental data for the turbulent coaxial jet under investigation, as demonstrated in Pinho (2020).

2.1.2 Dynamic Model of Germano - DSGS

To overcome some of limitations of Smagorinsky model, Germano *et al.* (1991) derived a dynamic subgrid-scale eddy viscosity model, using the concept of similarity of scales (Bardina *et al.*, 1980; Germano, 1990). This model uses the strain deformation field on two different scales, and spectral information of the field of large scales to extrapolate the strain on the small scales. The mathematical development is based on a double filtration process with two different characteristic lengths (Germano *et al.*, 1991; Lilly, 1992): the first is the LES filter already presented, and the second is called test filter, which is indicated by the hat symbol (according to Lilly (1992), it is recommended that $\widehat{\Delta} = 2\Delta$). The following equation is used to evaluate dynamically and locally an equivalent of the Smagorinsky constant $C_s\left(\mathbf{x}, t\right)$, which replaces C_s in Eq. 18:

$$C_s\left(\mathbf{x}, t\right) \quad = \quad \frac{1}{2}\frac{L_{ij}M_{ij}}{M_{ij}M_{ij}} \tag{21}$$

where

$$L_{ij} \quad = \quad \widehat{\left(\overline{\rho\widetilde{u_i}\widetilde{u_j}}\right)} - \frac{\left(\widehat{\overline{\rho\widetilde{u_i}}\,\overline{\rho\widetilde{u_j}}}\right)}{\widehat{\overline{\rho}}} \tag{22}$$

$$M_{ij} \quad = \quad \widehat{\Delta^2|\widetilde{S}|\widetilde{S}_{ij}} - \widehat{\Delta}^2|\widehat{\widetilde{S}}|\widehat{\widetilde{S}}_{ij} \tag{23}$$

The main limitation of the Smagorinsky model (use of an *ad hoc* constant) is then overcome. It should be pointed that the Eq. 21 can lead to negative values for $C_s\left(\mathbf{x}, t\right)$, reproducing the backscatter energy effect. To ensure stability, the $C_s\left(\mathbf{x}, t\right) \leq 0.17$ and $C_s\left(\mathbf{x}, t\right) \mid \mu_e \geq 0$ restrictions were imposed in the present work, as suggested by Sagaut (Sagaut, 2006).

2.1.3 Velocity Structure Function - VSF

Chollet and Lesieur (1981) developed a methodology to calculate turbulent viscosity in the Fourier space, with the objective of obtaining the energy spectrum for solved flow scales without using information from small scales. According to this method, the turbulent viscosity in the Fourier space can be calculated as

$$\nu_t\left(\kappa_c, t\right) \quad = \quad \nu_t{}^+\sqrt{\frac{E\left(\kappa_c, t\right)}{\kappa_c}} \tag{24}$$

where $\nu_t{}^+ = 0.267$ is a constant determined by the energy balance and $E\left(\kappa_c, t\right)$ is the energy spectrum. According to Batchelor (Batchelor, 1953) there is a correspondence between the energy spectrum $E\left(\kappa, t\right)$ and the so called velocity structure function $F_2\left(\mathbf{x}, \mathbf{r}, t\right)$, defined in physical space, such that

$$E\left(\kappa_c, t\right) \quad = \quad 0.03\Delta F_2\left(\mathbf{x}, \mathbf{r}, t\right), \tag{25}$$

where $F_2\left(\mathbf{x}, \mathbf{r}, t\right)$ is replaced by $F_{2t}\left(\mathbf{x}, \mathbf{r}, t\right)$, which is the the truncated second-order local velocity structure function that can be calculated in LES (Métais and Lesieur, 1992), defined by

$$F_{2t}\left(\mathbf{x}, \mathbf{r}, t\right) \quad = \quad \left\langle \|\mathbf{u}\left(\mathbf{x} + \mathbf{r}, t\right) - \mathbf{u}\left(\mathbf{x}, t\right)\|\right\rangle_{\|\mathbf{r}\|=\Delta} \tag{26}$$

on which the operator $\langle\rangle$ indicates the spatial average around the point $\mathbf{x}$ inside a sphere of radius $\mathbf{r}$. The combination of equations above results in

$$\nu_t\left(\mathbf{x}, \Delta, t\right) \quad = \quad 0.104C_K{}^{-3/2}\Delta\sqrt{F_{2t}\left(\mathbf{x}, \Delta, t\right)}. \tag{27}$$

The detailed development of the Velocity Structure Function approach is presented in Métais and Lesieur (1992). According to Lesieur (2012) the use of this model leads to good results for free shear flows, being less dissipative than the Smagorinsky model.

2.2 Numerical Details

Details of code implementation and numerical methodology are thoroughly presented in the introductory paper of PMLES (Pinho and Muniz, 2020). The PMLES solver was developed for running LES in mixed architectures employing GPU (graphic processing units) computing, which has becoming more popular in LES (Markesteijn and Karabasov, 2018; Terrana *et al.*, 2020).

In summary, the filtered equations (Eq. 17) are discretized by the finite difference method, using second-order schemes and a regular three-dimensional structured cartesian grid with uniform spacing. The use of a regular spaced grids
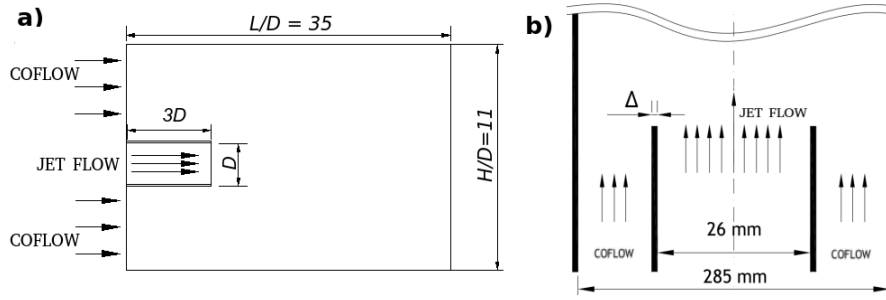
Figure 1. (a) Computational domain of the test problem and characteristic dimensions. (b) Characteristic dimensions and velocities ate the nozzle.

avoids the propagation of errors due to filter size variations (Piomelli, 1999; Ilyushin and Krasinsky, 2006). Temporal discretization was performed using a three-stage second-order Runge-Kutta scheme (Blazek, 2015), with a dimensionless time step of $\Delta t = 1.75 \times 10^{-4}$, which ensures CFL stability. We should note that use of an explicit scheme is quite efficient when working on a SIMT (*Single Instruction Multiple Thread*) architecture of GPU cards (Quadros, 2016), because it enables a massively parallel execution of thousands of threads independently and simultaneously (Ruetsch and Fatica, 2011). The pressure field for the incompressible flow is computed using the SOLA (SOLution Algorithm) method (Hirt *et al.*, 1975; Wilson *et al.*, 1988; Fortuna, 2000). The implementation was performed using CUDA Fortran programming to run on a suitable single workstation. Pinho and Muniz (2020) have shown that *speedups* of order of 55 are possible with this hybrid implementation.

2.3 Description of the test problem

To carry out the analysis, we chose the turbulent coaxial round jet described in Amielh *et al.* (1996) and Djeridane *et al.* (1996). A schematic description of the geometry of the experimental apparatus is shown in Fig. 1. The domain consists in a rectangular duct section with a circular coaxial duct for the high velocity fluid injection. Air at standard conditions flows in both ducts. The original setup has dimensions $L/D \simeq 50$ and $H/D \simeq 11$. Due to the high computational cost of the full problem, and considering that the analysis is focused on the near field, the length of computational domain was reduced to $L/D = 35$.

The computational domain was discretized using $N_x = 1004$ and $N_z = N_y = 317$ points, resulting on a regular mesh spacing of 3.49×10^{-2} and a domain with $\sim 1 \times 10^8$ cells. Despite using a Cartesian mesh, the circular injection duct of the jet was relatively well modeled. The momentum flux deviation by the cubic cells was evaluated and remained below 1 %.

The jet properties as defined in Fig. 1 are the same as in the experimental works (Amielh *et al.*, 1996; Djeridane *et al.*, 1996), i.e., inlet jet velocity $U_j = 12 \ m/s$, and coflow velocity $U_{coflow} = 0.09 \ m/s$, resulting in a Reynolds jet number of $Re = \frac{\rho U_j D}{\mu} = 20650$. The inlet boundaries and the rigid boundary walls (far from the regions of interest) are modeled by Dirichlet conditions, and a Neumann boundary condition for fully developed flows was applied at the outlet, assuming that the gradient of normal momentum flux is null. For the inlet jet zone, a fully developed velocity profile for circular duct Abramovich (1963) was set:

$$\frac{\widetilde{u}(r)}{\widetilde{u}_{max}} \quad = \quad \left(1 - \frac{r}{R}\right)^{1/7}. \tag{28}$$

For the coflow zone, a planar velocity profile was defined. In both inlet zones, the velocity fluctuations were not included.

3. RESULTS

The turbulent flow in the coaxial jet described in the previous section was simulated by LES using the three presented models for the subgrid-scale stress tensor. A comparison of results was done using profiles of time-averaged variables in the central plane (2D) and along the main axis and selected cross sections (1D). The variables used in the analysis were the dimensionless velocity U_{adm} and the dimensionless turbulence intensity u'_{adm}, defined as

$$U_{adm} = (U_L - U_{coflow})/(U_j - U_{coflow}), \tag{29}$$

$$u'_{adm} = u'_{rms}/(U_L - U_{coflow}) \tag{30}$$

where U_L is the local axial component of average velocity and u'_{rms} the root mean square velocity. These are computed by

$$U_L \quad = \quad \frac{\sum_{a=1}^{N} u_a}{N} \tag{31}$$

$$u'_{rms} = \sqrt{\frac{\sum_{a=1}^{N}(u_a - \langle\langle u\rangle\rangle)^2}{N}} \tag{32}$$

where u_a is a sample of the axial instantaneous velocity on a given point of the domain. The average values were calculated over $N = 300$ samples taken every 10000 steps of time after the steady regime is reached.

The analysis of the use of different SGS models to simulate the jet starts with a qualitative comparison of the average velocity fields depicted in Fig. 2. Visual inspection of these fields shows that the jet potential core length (the region with the highest velocities colored in dark red) was not significantly influenced by the use of different subgrid models. On the other hand, the behavior of the transition zone exhibited a greater sensitivity to the SGS model used. The transition zones of the jet predicted by the DSGS and VSF models are respectively the shortest and the longest. A more careful analysis of these fields indicate that the average velocities at $\sim x/D = 10$ in the simulation with the DSGS model are comparable to those observed at $\sim x/D = 15$ in the one performed with the VSM model, suggesting that the length of the transition zone predicted by the latter is about twice as long as that predicted by the DSGS model. The use of the Smagorinsky model predicted a jet with an intermediate potential core length.

These observations can be confirmed by analyzing the dimensionless axial velocity profiles along the main axis in Fig. 3, where also is plotted the experimental result of Amielh *et al.* (1996), the LES result of Wang *et al.* (2008) and the Similarity Law of jets of Chen and Rodi (1980). The three tested models indeed predict similar jet potential core lengths, considering that the transition zone starts in the axial position $\sim x/D = 6$ for all cases. On the other hand, each model represents the transition region in a different way as discussed before. The use of the DSGS model led to the highest spreading rate, indicated by the most significant reduction of U_{adm} in the central line, almost coinciding with the similarity law of Chen and Rodi Chen and Rodi (1980). This higher spreading rate is then responsible for the shorter transition zone. The VSF model led to the lowest spreading rate, while the Smagorinsky model ($C_s = 0.060$) presents an intermediate behavior, leading to a profile closer to the experimental results Amielh *et al.* (1996), with smaller deviations than the result of Wang *et al.* (2008).

A comparison between the turbulence intensity u'_{adm} profiles along the main axis predicted by the three SGS models is shown in Fig. 4. Again it is evident that the use of the DSGS model led to an earlier development of turbulence compared to the others, better predicting the jet regime transition behavior and the turbulence intensity after the transition. Also, the results clearly show the difficulty of the VSF model to predict the transition to turbulence, leading to the largest deviations with respect to the experimental data and other approaches from the literature. The results produced by the Smagorinsky model presented reasonable quantitative results, but good in qualitative terms. These variations on the development of turbulence corroborate the behavior of the three subgrid models with respect to the jet spreading rate discussed above.

In general, these results show that DSGS and VSF models predict respectively the shortest and longest transition zones and the highest and lowest spreading rates, while the Smagorinsky model presents an intermediate behavior, and exhibits the best agreement of the axial and radial profiles of average properties with the experimental data used in the analysis. A quantitative analysis of the performance of the three models evaluated is shown in Tab. 1, based on the mean squared errors MSE1 and MSE2 with respect to the experimental data Amielh *et al.* (1996), defined as

$$MSE1\left(\widehat{U_{adm}}\right) = \frac{1}{N}\sum_{a=1}^{N}\left[\left(\widehat{U_{adm}}\right)_a - (U_{adm})_a\right]^2 \tag{33}$$

$$MSE2\left(\widehat{u'_{adm}}\right) = \frac{1}{N}\sum_{a=1}^{N}\left[\left(\widehat{u'_{adm}}\right)_a - \left(u'_{adm}\right)_a\right]^2. \tag{34}$$

For MSE1, the lowest value was obtained for the simulation using the Smagorinsky model, while the lowest value of MSE2 was obtained for the simulation using the DSGS model. Therefore, based on this result and the full analysis discussed before, we can conclude that the Smagorinsky model better described the mean flow characteristics, while the DSGS model better predicted the turbulent characteristics and jet structure.

Table 1. Comparison between mean squared errors for simulations with different SGS models.

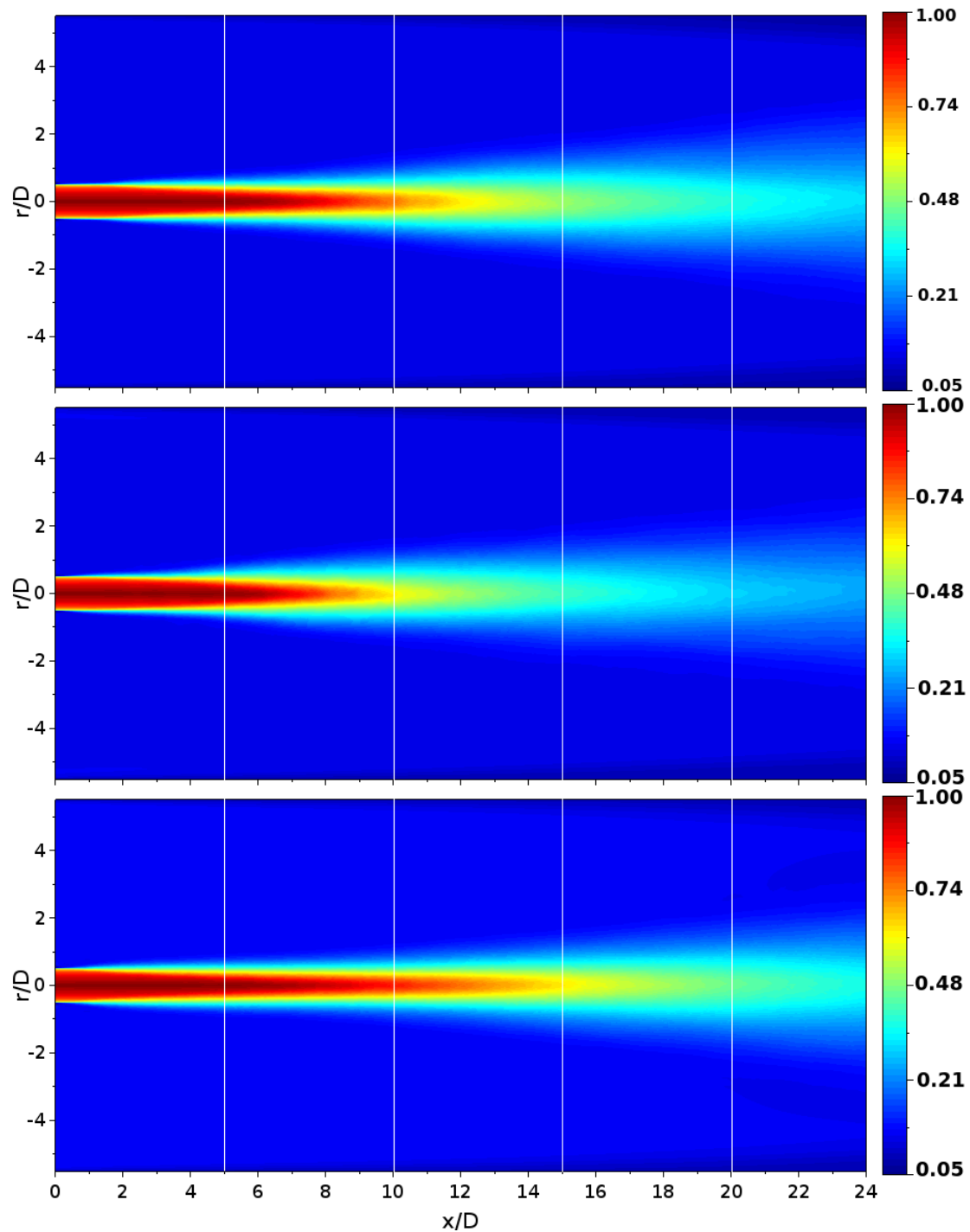| SGS model	MSE1($\times 10^3$)	MSE2($\times 10^3$)
Smagorinsky ($C_s = 0.060$)	1.65	1.70
DSGS	4.72	0.56
VSF	10.30	4.41

Figure 2. Average dimensionless axial velocity fields computed by simulations with the a) Smagorinsky ($C_s = 0.060$), b) DSGS and c) VSF models.
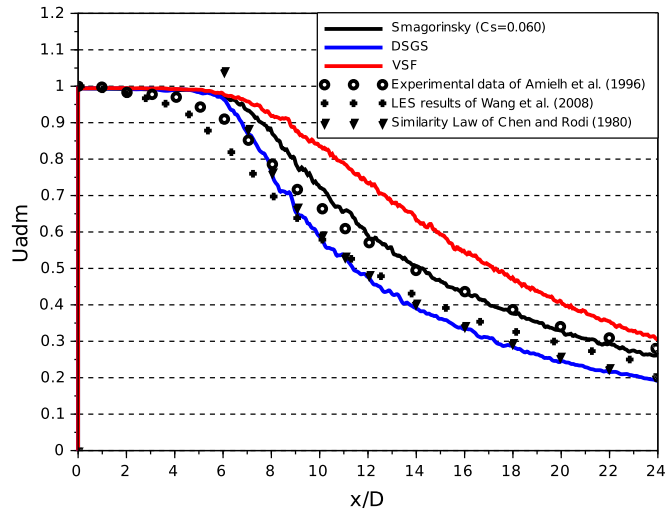
Figure 3. Profiles for dimensionless velocity U_{adm} along the main axis obtained with different SGS models, compared to literature data Amielh *et al.* (1996); Wang *et al.* (2008); Chen and Rodi (1980).
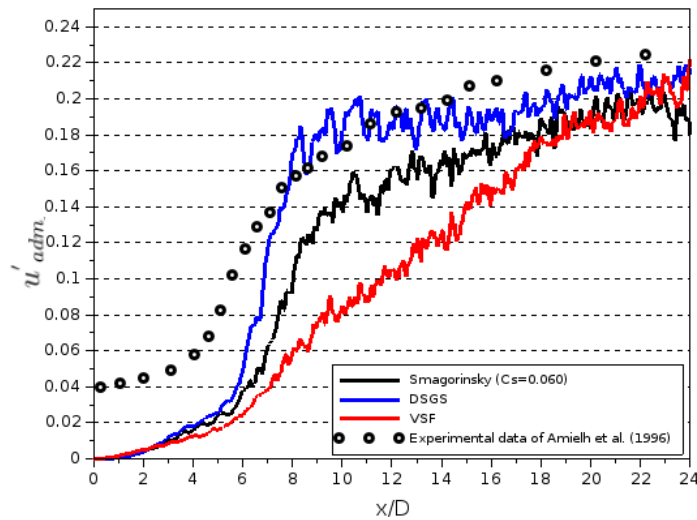

Figure 4. Profiles for dimensionless turbulence intensity u'_{adm} along the main axis obtained with different SGS models, compared to literature data Amielh *et al.* (1996).

4. CONCLUSIONS

The main objective of this work was to evaluate the effect of subgrid-scale modeling of stress tensor in LES of a turbulent coaxial jet. Simulations were performed using three SGS models (Smagorinsky, DSGS and VSF) and results were compared to experimental data and other numerical results from the literature. The results showed that the Smagorinsky subgrid model with $C_s = 0.060$ (value chosen in the analysis of Pinho (2020)), led to the smallest deviations for the average velocities with respect to the experimental data. The dynamic model of Germano was the one that best described the turbulent characteristics of the jet, even though it led to higher mean quadratic errors for the average values compared to the Smagorinsky model, in addition to being computationally more expensive (about 21%). The transition to turbulence and spreading rate was more suitably predicted by this method. The use of the Velocity Structure Function model did not produce reasonable results in our case. According to Lesieur Lesieur *et al.* (2005), this model is indicated to simulate flows where there is a transition to turbulence, however in our simulations the model did not show a good capacity to capture this transition and consequently the transition of jet regimes.

This work demonstrates that a performance analysis of the existing models is an important step in the development of new models for LES and their application in problems of interest, and that the most computationally expensive and complex model may not be always the best choice. Then, in view of the results of this work and previous studies in the literature, it is suggested that for LES of an unknown problem involving transition from laminar to turbulent flow,

the DSGS model should be used. When the objective is to obtain reliable solutions at a cheaper cost to study a particular phenomenon (involving heat or mass transfer, for example), it may be worth looking for an adequate value of the Smagorinsky constant C_s before its application.

Throughout the development of this work, we found that there are many important questions to be answered in the LES context of turbulent jets. Although we know that it does not make sense to talk about mesh refinement it is interesting to analyze the sensitivity of the simulations regarding the mesh used so that a clear mesh choice criterion can be built. Apply methodologies to describe the turbulent inlet condicios and reassess the performance of the models, as it is possible that these influence the performance of the models. Analyse the performance of the models tested here for other jets, in order to assess the sensitivity of the performance of the sub-mesh models in terms of flow conditions.

5. ACKNOWLEDGEMENTS

6. REFERENCES

Abramovich, G., 1963. *The theory of turbulent jets*. Ph.D. thesis, MIT Press, Massachusetts Institute of technology.

Amielh, M., Djeridane, T., Anselmet, F. and Fulachier, L., 1996. "Velocity near-field of variable density turbulent jets". *International Journal of Heat and mass transfer*, Vol. 39, No. 10, pp. 2149–2164.

Bardina, J., Ferziger, J.H. and Reynolds, W.C., 1980. "Improved subgrid-scale models for large-eddy simulation". In *American Institute of Aeronautics and Astronautics, Fluid and Plasma Dynamics Conference, 13th, Snowmass, Colo., July 14-16, 1980, 10 p.*

Batchelor, G.K., 1953. *The theory of homogeneous turbulence*. Cambridge university press.

Blazek, J., 2015. *Computational fluid dynamics: principles and applications*. Butterworth-Heinemann.

Bodony, D.J. and Lele, S.K., 2008. "Current status of jet noise predictions using large-eddy simulation". *AIAA journal*, Vol. 46, No. 2, pp. 364–380.

Brès, G.A. and Lele, S.K., 2019. "Modelling of jet noise: a perspective from large-eddy simulations". *Philosophical Transactions of the Royal Society A*, Vol. 377, No. 2159, p. 20190081.

Chen, C.J. and Rodi, W., 1980. "Vertical turbulent buoyant jets: a review of experimental data". *NASA Sti/Recon Technical Report A*, Vol. 80.

Chollet, J.P. and Lesieur, M., 1981. "Parameterization of small scales of three-dimensional isotropic turbulence utilizing spectral closures". *Journal of the Atmospheric Sciences*, Vol. 38, No. 12, pp. 2747–2757.

Djeridane, T., Amielh, M., Anselmet, F. and Fulachier, L., 1996. "Velocity turbulence properties in the near-field region of axisymmetric variable density jets". *Physics of Fluids*, Vol. 8, No. 6, pp. 1614–1630.

Fortuna, A.d.O., 2000. *Técnicas computacionais para dinâminca dos fluidos: conceitos básicos e aplicações*. Edusp.

Germano, M., 1990. "Averaging invariance of the turbulent equations and similar subgrid scale modeling". *CTR Manuscript*, Vol. 116.

Germano, M., Piomelli, U., Moin, P. and Cabot, W.H., 1991. "A dynamic subgrid-scale eddy viscosity model". *Physics of Fluids A: Fluid Dynamics*, Vol. 3, No. 7, pp. 1760–1765.

Hirt, C. *et al.*, 1975. "Sola: A numerical solution algorithm for transient fluid flows". Technical report, Los Alamos Scientific Lab., N. Mex.(USA).

Huai, Y., 2006. *Large Eddy Simulation in the scalar field*. Ph.D. thesis, Technische Universität.

Ilyushin, B. and Krasinsky, D., 2006. "Large eddy simulation of the turbulent round jet dynamics". *Thermophysics and Aeromechanics*, Vol. 13, No. 1, pp. 43–54.

Kuo, K.K.y. and Acharya, R., 2012. *Fundamentals of Turbulent and Multi-Phase Combustion*. John Wiley & Sons.

Lesieur, M., 2012. *Turbulence in fluids*, Vol. 40. Springer Science & Business Media.

Lesieur, M., Métais, O. and Comte, P., 2005. *Large-eddy simulations of turbulence*. Cambridge University Press.

Lilly, D.K., 1992. "A proposed modification of the germano subgrid-scale closure method". *Physics of Fluids A: Fluid Dynamics*, Vol. 4, No. 3, pp. 633–635.

Löffler, M., Pfadler, S., Beyrau, F., Leipertz, A., Dinkelacker, F., Huai, Y. and Sadiki, A., 2008. "Experimental determination of the sub-grid scale scalar flux in a non-reacting jet-flow". *Flow, Turbulence and Combustion*, Vol. 81, No. 1, pp. 205–219.

Markesteijn, A.P. and Karabasov, S.A., 2018. "GPU CABARET solutions for the cojen jet noise experiment". In *2018 AIAA/CEAS Aeroacoustics Conference*. p. 3921.

Métais, O. and Lesieur, M., 1992. "Spectral large-eddy simulation of isotropic and stably stratified turbulence". *Journal of Fluid Mechanics*, Vol. 239, pp. 157–194.

Moin, P., Squires, K., Cabot, W. and Lee, S., 1991. "A dynamic subgrid-scale model for compressible turbulence and

scalar transport". *Physics of Fluids A: Fluid Dynamics*, Vol. 3, No. 11, pp. 2746–2757.

Pierce, C.D. and Moin, P., 2004. "Progress-variable approach for large-eddy simulation of non-premixed turbulent combustion". *Journal of Fluid Mechanics*, Vol. 504, pp. 73–97.

Pierce, C.D., 2001. *Progress-variable approach for large-eddy simulation of turbulent combustion*. Ph.D. thesis, stanford university.

Pinho, J.M.d., 2020. *O Efeito da Modelagem Submalha em Simulações de Grandes Escalas de Jatos Coaxiais Turbulentos*. Ph.D. thesis, Universidade Federal do Rio Grande do Sul.

Pinho, J. and Muniz, A.R., 2020. "PMLES: A hybrid openMP CUDA source code for LES of turbulent flows". *Journal of Applied Fluid Mechanics*, Vol. 13, No. 4, pp. 1067–1079.

Piomelli, U., 1999. "Large-eddy simulation: achievements and challenges". *Progress in Aerospace Sciences*, Vol. 35, No. 4, pp. 335–362.

Pope, S.B., 2000. *Turbulent flows*. Cambridge university press.

Quadros, A.E.R., 2016. *Processamento Paralelo em CUDA Aplicado ao Modelo de Geração de cenários sintéticos de vazões e Energias-GEVAZP*. Ph.D. thesis, Universidade Federal do Rio de Janeiro.

Ruetsch, G. and Fatica, M., 2011. "Cuda fortran for scientists and engineers". *NVIDIA Corporation*, Vol. 2701.

Sagaut, P., 2006. *Large eddy simulation for incompressible flows: an introduction*. Springer Science & Business Media.

Schmitt, F.G., 2007. "About boussinesq's turbulent viscosity hypothesis: historical remarks and a direct evaluation of its validity". *Comptes Rendus Mécanique*, Vol. 335, No. 9-10, pp. 617–627.

Silva Freire, A.P., Menut, P.P.M. and Jian, S., 2002. *Turbulência*, Vol. 1. ABCM.

Smagorinsky, J., 1963. "General circulation experiments with the primitive equations: I. the basic experiment". *Monthly weather review*, Vol. 91, No. 3, pp. 99–164.

Tennekes, H. and Lumley, J.L., 1972. *A first course in turbulence*. MIT press.

Terrana, S., Nguyen, C. and Peraire, J., 2020. "Gpu-accelerated large eddy simulation of hypersonic flows". In *AIAA Scitech 2020 Forum*. p. 1062.

Wang, P., Fröhlich, J., Michelassi, V. and Rodi, W., 2008. "Large-eddy simulation of variable-density turbulent axisymmetric jets". *International Journal of Heat and Fluid Flow*, Vol. 29, No. 3, pp. 654–664.

Wilson, T. *et al.*, 1988. "Sola-dm: A numerical solution algorithm for transient three-dimensional flows". Technical report, Los Alamos National Lab.

7. RESPONSIBILITY NOTICE

The authors are the only responsible for the printed material included in this paper.